UDK 54.057:544.022.822
Original scientific article/Izvirni znanstveni članek

ISSN 1580-2949
Mater. Tehnol.

# COMPONENT OPTIMIZATION OF g-$C_3N_4$/$TiO_2$ HETEROSTRUCTURE COMPOSITE AND ITS ACTIVITY ENHANCEMENT FOR PHOTOCATALYTIC DEGRADATION OF RHODAMINE B

## OPTIMIZACIJA KOMPONENT KOMPOZITNE HETEROSTRUKTURE g-$C_3N_4$/$TiO_2$ IN POVEČANJE NJENE AKTIVNOSTI ZA FOTOKATALITSKO RAZGRADNJO RODAMINA B

**Zikang Cao,[1] Yating Liu,[1] Luqi Wang,[1] Xu Gao,[1] Sitian Chen,[1] Sitian Cheng,[1] Yan Yu,[2,3*] Li Li[1, 2]**

[1]College of Chemistry and Chemical Engineering, Qiqihar University, Qiqihar, Heilongjiang 161006, China
[2]College of Materials Science and Engineering, Qiqihar University, Qiqihar, Heilongjiang 161006, China
[3]Heilongjiang Provincial Key Laboratory of Polymeric Composition Materials, Qiqihar, Heilongjiang 161006, China

*Prejem rokopisa – received: 2024-07-19; sprejem za objavo – accepted for publication: 2024-12-05*

doi:10.17222/mit.2024.1251

In this study, g-$C_3N_4$/$TiO_2$ heterostructure composites were synthesized using sol–gel and hydrothermal methods. Through X-ray powder diffraction (XRD) and X-ray photoelectron spectroscopy (XPS), the crystalline phase structure and chemical composition of the composite were confirmed. Scanning electron microscopy (SEM) revealed that the g-$C_3N_4$ sheets were uniformly dispersed on the block $TiO_2$ particles. Ultraviolet–visible diffuse reflectance spectroscopy (UV–Vis/DRS) indicated that the incorporation of g-$C_3N_4$ resulted in a narrowing of the forbidden bandwidths of the composites. Photoluminescence (PL) spectroscopy and electrochemical impedance spectroscopy (EIS) further demonstrated that the g-$C_3N_4$/$TiO_2$ heterostructure effectively suppressed the recombination of photogenerated charge carriers. To evaluate the photocatalytic performance of g-$C_3N_4$/$TiO_2$ heterojunction composites, different g-$C_3N_4$ loadings were tested for degradation of rhodamine B (RhB). The 7.62 *w*/% g-$C_3N_4$/$TiO_2$ heterojunction composite exhibited the highest degradation efficiency for RhB dye, with a constant degradation rate that was twice as high as that of pure $TiO_2$. Additionally, experiments on free radical trapping of the composite revealed the crucial role of hydroxyl radicals (·OH) and photogenerated holes ($h^+$) in the RhB degradation. Moreover, the formation of a Z-scheme heterojunction between g-$C_3N_4$ and $TiO_2$ was the main factor in further enhancing the degradation activity of the composite.

Keywords: hydrothermal synthesis, g-$C_3N_4$, $TiO_2$, photocatalysis

V članku avtorji opisujejo izdelavo hetero-strukturiranega kompozita g-$C_3N_4$/$TiO_2$, ki je bil sintetiziran s sol-gel postopkom in hidrotermalno metodo. Kristalno fazno strukturo in kemično sestavo kompozitov so avtorji določili z rentgensko praškovno difrakcijo (XRD) in rentgensko fotoelektronsko spektroskopijo (XPS). Analiza z vrstično elektronsko mikroskopijo (SEM) je pokazala, da so luske g-$C_3N_4$ enakomerno porazdeljene po površini delcev $TiO_2$. Difuzijska odbojna spektroskopija v ultravijolični in vidni svetlobi (UV-Vis/DRS) je pokazala, da vključitev g-$C_3N_4$ povzroči zožitev širine prepovedanega pasu kompozitov. Fotoluminiscenčna spektroskopija (PL) in elektrokemijska impedančna spektroskopija (EIS) sta pokazali, da heterostruktura g-$C_3N_4$/$TiO_2$ učinkovito zavira rekombinacijo fotogeneriranih nosilcev naboja. Avtorji raziskave so ugotavljali tudi vpliv različnih vsebnosti g-$C_3N_4$ na razgradnjo rodamina B (RhB), da bi ocenili fotokatalitično učinkovitost kompozitov g-$C_3N_4$/$TiO_2$ s hetero priključkom. Pri tem so kompoziti g-$C_3N_4$/$TiO_2$ s 7,62 wt.% pokazali najvišjo učinkovitost razgradnje barvila RhB. Ugotovili so, da je bila konstanta hitrosti razgradnje dvakrat višja kot pri čistem $TiO_2$. Poleg tega so poskusi lovljenja prostih radikalov v kompozitu pokazali, da imajo hidroksilni radikali (OH) in fotogenerirane luknje ($h^+$) ključno vlogo v procesu razgradnje RhB in, da je nastanek heteroprehoda tipa Z med g-$C_3N_4$ in $TiO_2$ glavni dejavnik za nadaljnje povečanje aktivnosti razgradnje kompozita.

Ključne besede: hidrotermalna sinteza, g-$C_3N_4$, $TiO_2$, fotokataliza

## 1 INTRODUCTION

Dyes are widely used in the leather, textile, and dyeing sectors, and water pollution has progressively grown to be a major environmental concern for humankind.[1–3] This is mostly due to several hazardous chemicals present in dye wastewater that obstruct photosynthesis and oxygen consumption, which has a negative impact on the ability of aquatic species to grow and survive. On the other hand, according to prior research, humans who consume or are subjected to contaminated water at extremely low concentrations for an extended period may suffer from many kinds of physical illnesses, including cancer.[4]

Semiconductor photocatalysis is an efficient environmental cleaning technology that can completely decompose organic pollutants into environmentally benign substances such as water ($H_2O$), carbon dioxide ($CO_2$), and inorganic salts.[5] The catalytic degradation of organic pollutants can be achieved under mild reaction conditions, with complete degradation and no secondary pollution occurring when sunlight is applied at room temperature

*Corresponding author's e-mail:
zglnasyy@163.com (Yan Yu)

and pressure. Because of its exceptional chemical and biological stability, inherent catalytic degradation capacity, nontoxicity, and environmental friendliness, $TiO_2$ is regarded as one of the most acceptable photocatalytic semiconductor materials suitable for the photocatalytic degradation of organic pollutants and toxic substances.[6,7] However, $TiO_2$ has limited performance in visible and infrared photoresponses because of its large energy band gap ($E_g$ = 3.2 eV) and rapid recombination of photogenerated carriers, significantly hindering its photocatalytic efficiency in widespread applications.[8] Therefore, $TiO_2$ semiconductor photocatalysts must be modified to enhance their photocatalytic activity. Generally, enhancing the photocatalytic activity of $TiO_2$ through the creation of semiconductor heterostructures is an easy and useful method that not only enhances spectral absorption but also prevents the recombination of photogenerated electron–hole pairs.

So far, significant efforts have been dedicated to improving the photocatalytic efficiency of $TiO_2$, for example, by doping it with metallic or nonmetallic elements,[9] with surface modification,[10] and semiconductor coupling by forming heterojunctions.[11] Nevertheless, the majority of these require expensive raw materials (e.g., rGO, $MoS_2$, and noble metals). Therefore, logically altering the structure of $TiO_2$ to quicken the separation of photogenerated carriers and increase the photoresponsive range in an economical and nontoxic way is essential for overcoming this dilemma.

For the past few years, graphitic-phase carbon nitride (g-$C_3N_4$) has gained significant attention as a promising material for modifying semiconductor photocatalysts.[12] g-$C_3N_4$ is a novel photocatalyst with a narrow band gap of 2.7 eV and a strong spectral response to visible light. However, the photocatalytic effectiveness of pure g-$C_3N_4$ is constrained by the ease with which its photogenerated electron–hole pairs form complexes. Based on relevant literature, g-$C_3N_4$ and $TiO_2$ can work together to effectively boost the visible-light response, leading to satisfactory photocatalytic efficiency. This is because their bandgaps are well matched, and creating heterojunction interfaces at the boundaries is easy.[13,14] For example, Lv et al.[15] reported that g-$C_3N_4$ effectively removed the photogenerated electrons accumulating on a high-energy $TiO_2$ (101) crystalline surface, leading to the generation of spatially isolated photogenerated holes and electrons, thereby increasing the photocatalytic activity. Li et al[16] synthesized g-$C_3N_4$/$TiO_{2-x}N_y$ composites by incorporating platinated titania and platinated titanite–rutile with N-doped $TiO_2$ nanoparticles. They used $TiCl_3$ as a source of Ti. The addition of rutile–phase $TiO_{2-x}N_y$ effectively transfers photogenerated electrons from rutile $TiO_2$ to g-$C_3N_4$, improving electron–hole pair separation efficiency and augmenting the photocatalytic activity. However, alkoxylated titanium, organic solvents, or stringent conditions are usually used in the preparation of these g-$C_3N_4$/$TiO_2$ complexes.[17] Therefore, there is an urgent need to explore a relatively economical method for preparing g-$C_3N_4$/$TiO_2$ composites with a structurally stable, homogeneous morphology, large specific surface area, and heterogeneous structure.[18–21]

Accordingly, we synthesized g-$C_3N_4$/$TiO_2$ heterojunction photocatalytic composites through sol-gel and hydrothermal methods. The morphology and structural properties of the composites were characterized with analytical methods including XPS, XRD, SEM, PL, UV-Vis/DRS, EIS, and $N_2$ adsorption-desorption. The photocatalytic performance of the g-$C_3N_4$/$TiO_2$ heterojunction composites was estimated using the typical RhB dye, and reactive species trapping experiments were executed to probe the effect of the heterojunction on the photocatalytic degradation system, determining a possible mechanism of the photocatalytic reaction.

## 2 EXPERIMENTAL PART

### *2.1. Materials and instruments*

Tetraisopropyl orthotitanate ($C_{12}H_{28}O_4Ti$, AR grade, ≥97.0%); Melamine ($C_3H_6N_6$, AR grade, ≥99.0%); Poly(ethylene glycol)-block-poly(propylene glycol)-block-poly(ethylene glycol) (P123) ($C_{18}H_{36}O_5X_2$, AR grade); Rhodamine B (RhB) ($C_{28}H_{31}ClN_2O_3$, AR grade); Methanol ($CH_3OH$, AR grade, ≥99.5%); Ethanol ($C_2H_5OH$, AR grade, ≥99.7%); P-benzoquinone (BQ) ($C_6H_4O_2$, AR grade); Disodium ethylenediaminetetraacetic acid (EDTA-2Na) ($C_{10}H_{14}N_2Na_2O_8$, AR grade); Isopropyl alcohol (IPA) ($C_3H_8O$, AR grade, ≥99.7%). The reagents used in the experiments were not further purified, and the experimental water used was deionized water.

XRD spectra of the samples were analyzed with a Bruker-AXS (D8) X-ray diffractometer, Germany. The measurements were conducted with a Cu target, K$\alpha$ radiation ($\lambda$ = 0.15406 nm), a scanning range of 5–90°, scanning speed of 1 °/min, working voltage of 40 kV, and working current of 180 mA. The surface valence states of the samples were determined using a VGADES400 X-ray photoelectron spectroscopy (XPS) instrument, with Mg K$\alpha$ radiation (h$\nu$ = 1486.4 eV) as the excitation source. The vacuum level was maintained at $10^{-8}$ Pa, and the data were calibrated using the linear mode. The morphology of the samples was analyzed using a Hitachi S-4700 scanning electron microscope (SEM) with an operating voltage of 5 kV. The photoluminescence (PL) spectra of the samples were measured using a Hitachi F-7000 fluorescence spectrophotometer. The electrochemical impedance spectroscopy (EIS) of the samples was conducted using a PEC-1000 photoelectrochemical testing system produced by Bio-Logic. The specific surface area and pore size of the samples were measured using a 3H-2000 specific surface area and pore size analyzer from Beijing Beishide Company at a temperature of 77 K. The UV-visible absorption spectra of the samples in a wavelength range of 200–800 nm were recorded

using a TU-1901 UV–Vis double-beam spectrophotometer from Beijing Puxi General Analysis Co., Ltd. $BaSO_4$ was used as the reference. The absorbance of the sample solution was determined using a TU-1901 UV–Vis double-beam spectrophotometer produced by Beijing Puxi General Analysis Co., Ltd.

### *2.2 Preparation of g-$C_3N_4$ /$TiO_2$ composites*

Preparation of g-$C_3N_4$ was conducted as follows: g-$C_3N_4$ was synthesized through thermal polymerization. A specific quantity of melamine was measured and subjected to calcination at 550 °C for 4 h in a crucible. Afterwards, it was cooled to room temperature and milled to produce powdered g-$C_3N_4$ solid, which was named CN.

Preparation of g-$C_3N_4$/$TiO_2$ composite materials: Ultrasonically, various concentrations of g-$C_3N_4$ were dispersed in 10 mL of isopropanol. Two milliliters of tetraisopropyl titanate were added, and the mixture was stirred magnetically for 30 min or until it was thoroughly combined. After adding 0.6 mL of P123 and stirring the mixture rapidly for 30 min, the solution was allowed to completely dissolve. Deionized water was added gradually to the mixed solution, and the mixture was stirred until a pale-yellow colloid formed. Finally, after a solid gel was formed by slow stirring, the gel was transferred to a polytetrafluoroethylene reactor, and the temperature was increased to 200 °C for 2 h. The collected solid was separated by centrifugation and then rinsed multiple times with deionized water and ethanol. The g-$C_3N_4$/$TiO_2$ composite materials were created with varying weight ratios of g-$C_3N_4$ (6.51, 7.62, 8.49, 12.37, and 19.60 %) and labelled as 6.51 *w*/% CN/T, 7.62 *w*/% CN/T, 8.49 *w*/% CN/T, 12.37 *w*/% CN/T, and 19.60 *w*/% CN/T, respectively.

### *2.3 Photocatalysis experiments*

The photocatalytic degradation performance of the prepared samples was evaluated using the decolourisation results of the RhB solution. Firstly, 150 mg of the photocatalyst was completely dispersed in 90 mL (50 mg/L) of an RhB solution, and the suspension was placed in dark conditions for 30 min to achieve adsorption-desorption equilibrium. Then the samples were exposed to an Xe lamp (MC-PF300, 300 W, Beijing Merry Change Technology Co, Ltd) for a certain time. The solutions were extracted at certain intervals and then centrifuged. The corresponding absorbance values were measured by a UV–Vis spectrophotometer (TU-1901 type), and the degradation rate was calculated using formula $C_t/C_0 = A_t/A_0$, where $C_0$ and $A_0$ are the concentration and absorbance value of the simulated pollutant before the light exposure, respectively, while $C_t$ and $A_t$ are the concentration and absorbance value of RhB at the photocatalytic time of $t$ min. The reaction device for the UV light photocatalysis experiment was custom-made, featuring a built-in 125 W high-pressure mercury lamp with an emission wavelength of 313.2 nm. The photocatalytic reaction was cooled by circulating water directed to the reaction device.

## 3 RESULTS AND DISCUSSIONS

### *3.1 XRD analysis*

To investigate the crystalline structure of the CN/T composites, XRD analyses were performed on the CN and CN/T composites, and the corresponding results are shown in **Figure 1**. As shown in this figure, diffraction peaks at 25.46°, 37.88°, 48.02°, 54.14°, 54.86°, 62.71°, 75.31°, and 82.82° for pure $TiO_2$ can be attributed to (101), (004), (200), (105), (211), (204), (215) and (224) crystal planes, which is in accordance with $TiO_2$ (JCPDS 21-1272) from the literature.[22] For pure CN, there is a distinct characteristic peak at diffraction angle 2$\theta$ of 27.63°. This is consistent with the formation of graphite interlayer structures, which correspond to the (002) crystalline facets formed by the interlayer accumulation of aromatic hydrocarbon rings.[23] Diffraction peaks of the CN/T composite are mainly located at 25.46°, 37.88°, 48.02°, 54.14°, 54.86°, 62.71°, 75.31° and 82.82°, and they are consistent with the (101), (004), (200), (105), (211), (204), (215) and (224) crystal planes of anatase $TiO_2$ (JCPDS 21-1272), demonstrating the presence of anatase $TiO_2$ in the composite. In addition, the CN/T composite exhibited a weak diffraction peak at 27.40°, demonstrating its alignment with the (200) crystal plane of g-$C_3N_4$, indicating that the composite existed in both the crystalline phases of g-$C_3N_4$ and $TiO_2$ components. However, since the amount of CN in the composite is relatively small, the characteristic peak associated with the (200) crystal plane of g-$C_3N_4$ is not very obvious, indicating that $TiO_2$ hybridization with CN does not alter its diffraction peak crystal structure.[24] In addition, the absence of additional diffraction peaks fully proves that the

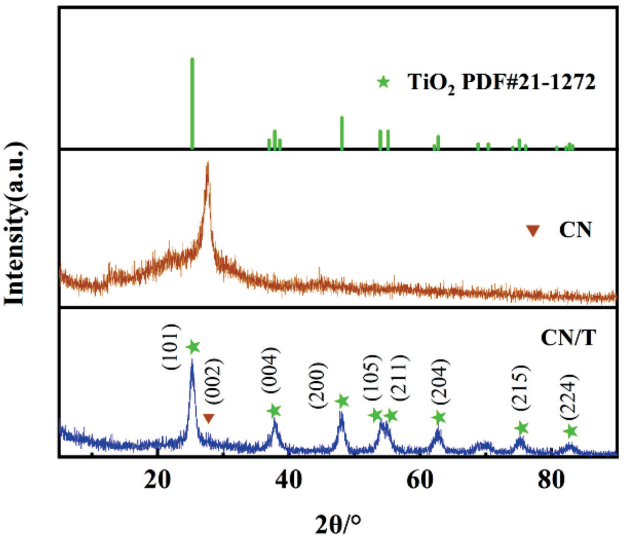


**Figure 1:** X-ray diffraction patterns of CN and CN/T

synthesized samples are of high purity without any by-products.

### *3.2 XPS analysis*

The surface composition and chemical valence states of CN/T composites were analyzed through XPS. The findings are illustrated in **Figure 2**. The full spectrum of **Figure 2a** clearly illustrates the presence of Ti, N, C, and O in the CN/T composite.[25] The C 1s high-resolution spectrum of CN/T is shown in **Figure 2b**, and three binding energy peaks at 284.9 eV, 286.4 eV and 288.7 eV are fitted, corresponding to the $sp^2$ hybridized carbons of the sample surface indeterminate carbons C–C, the carbons in the –C–$NH_x$ moiety, and the N–C=N bonds in the triazine ring structure, respectively.[26] Similarly, from the high-resolution spectra of the N 1s of CN/T in **Figure 2c**, the binding energies are located at 398.6 eV, 400.2 eV and 401.6 eV, corresponding to the $sp^2$ hybridized N species (C–N=C) and the tertiary N species (N–$(C)_3$-terminal C–$NH_x$ group), respectively, all of which are characteristic of the neutralization of the N atoms in CN, indicating the structural stability of CN.[27] The O 1s XPS spectra for CN/T composites are displayed in **Figure 2d**. These spectra display combined signals of hydroxyl-oxygen groups (531.9 eV) on the Ti–OH surface and Ti–O–Ti bonds (529.8 eV) formed by $TiO_2$ with adsorbed oxygen on the CN surface, which strongly suggests that CN and $TiO_2$ interactions exist.[28] **Figure 2e** shows two electronic states resulting from spin-orbit interactions corresponding to the two peaks of Ti $2p_{3/2}$ and Ti $2p_{1/2}$ at 459.8 eV and 465.6 eV, respectively,[29] suggesting a unique presence of $Ti^{4+}$. The XPS findings provided tentative verification of the heterojunction composite structure of $TiO_2$ and CN.

### *3.3 SEM analysis*

The microstructure and surface morphology of the prepared materials were examined by analyzing CN/T through SEM. **Figure 3** presents the findings. Compared with the bulk structure of $TiO_2$ nanoparticles shown in **Figures 3a–b**, **Figures 3c–d** demonstrate that CN is a sheet-like structure and $TiO_2$ nanoparticles are scattered on the surface of CN sheets in the composite; moreover, the aggregated CN nanosheets form a porous structure in the CN/T composites. The agglomeration of $TiO_2$ increases the roughness of CN nanosheets and is anticipated to improve the degradation ability of composites. The SEM analysis further confirmed that the prepared composite components were in close contact with each other and formed a heterogeneous structure between $TiO_2$ and CN, which was anticipated to enhance the degradation efficiency of CN/T composites.[30]

### *3.4 $N_2$ adsorption–desorption analysis*

$N_2$ adsorption and desorption measurements were performed on $TiO_2$, CN, and various compositions of CN/T composites to examine the physicochemical properties of the composite surfaces.

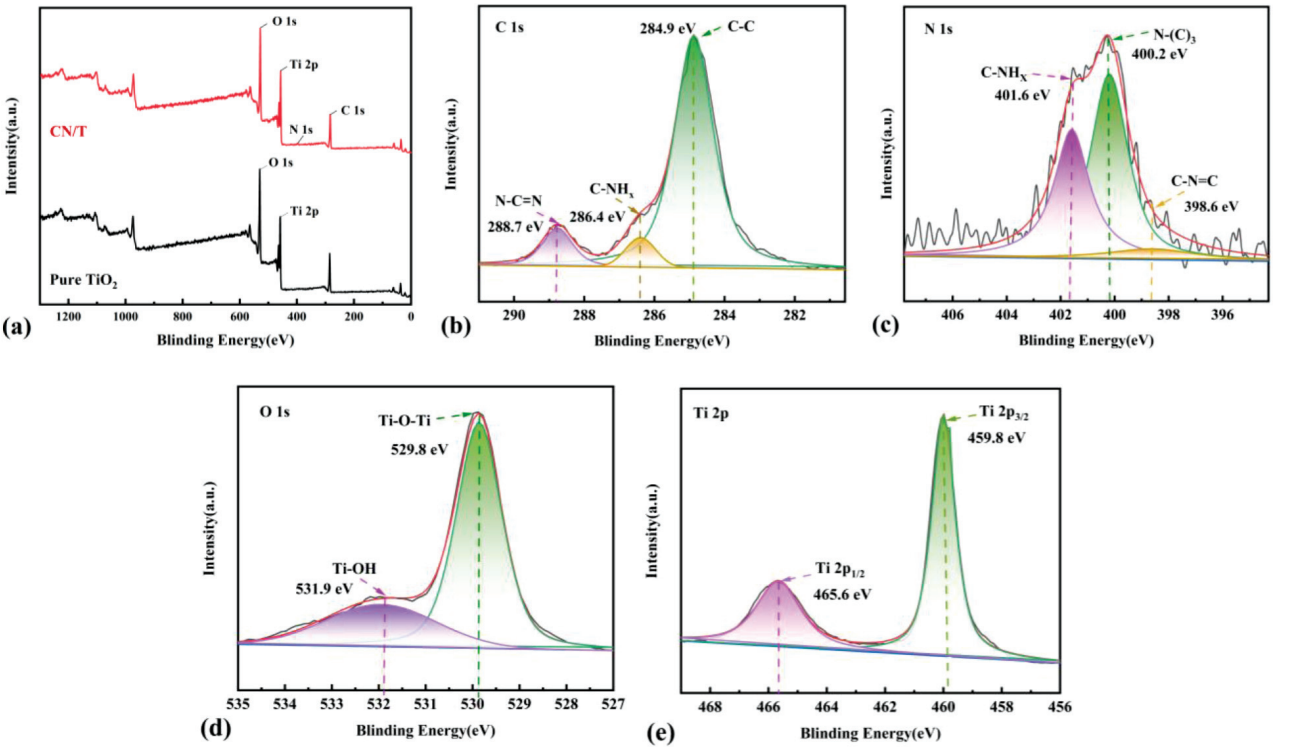


**Figure 2:** a) Full spectra of $TiO_2$ and CN/T, b) XPS spectra of C 1s, c) N 1s, d) O 1s and e) Ti 2p of CN/T

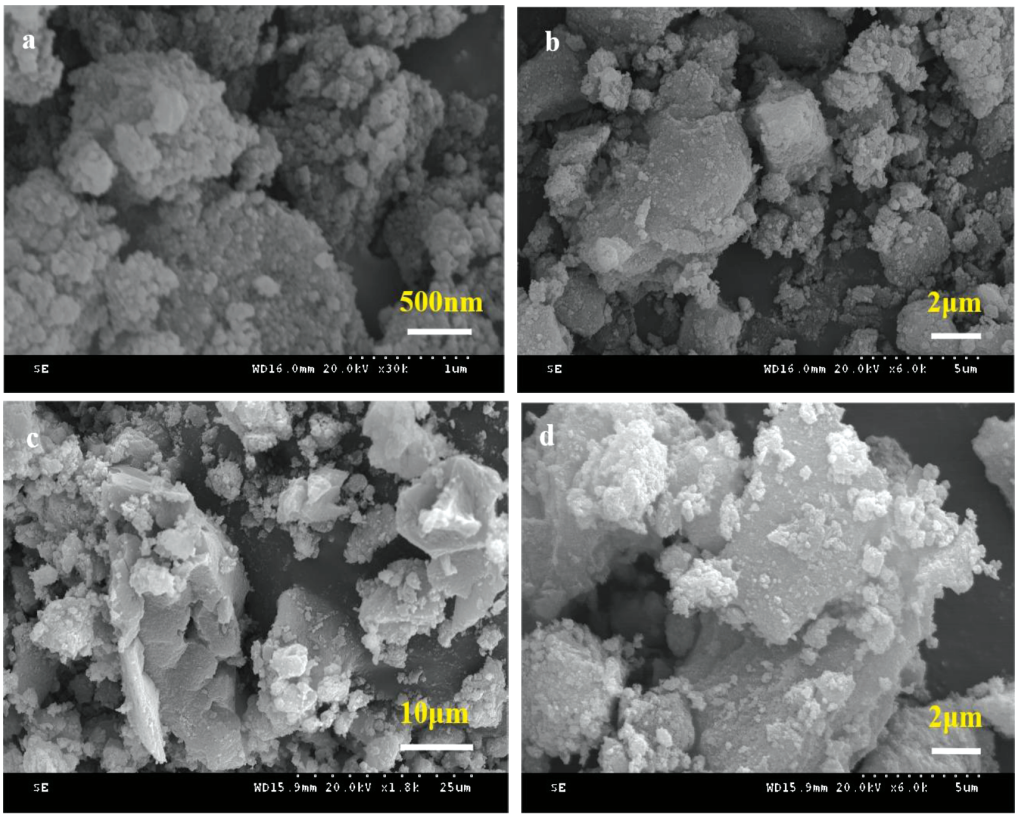


**Figure 3:** a), b) SEM images of $TiO_2$ and c), d) CN/T

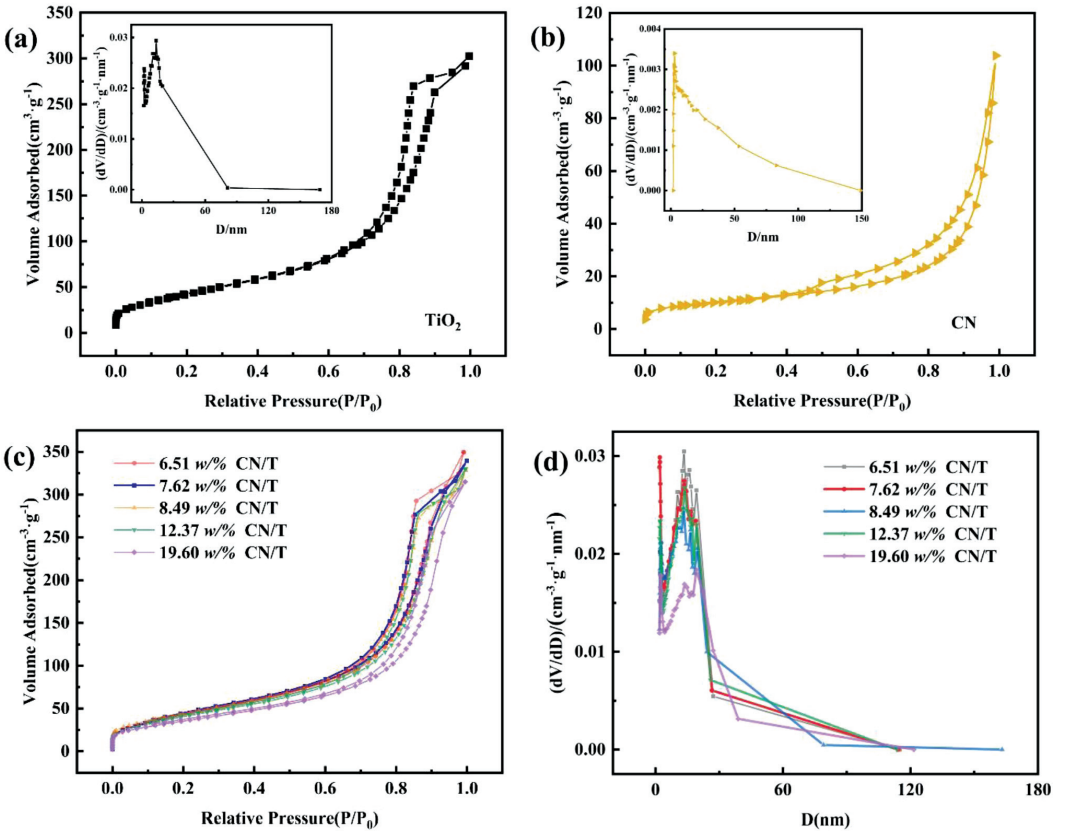


**Figure 4:** a) $N_2$ adsorption–desorption isotherms of $TiO_2$, b) CN (the inset is the BJH pore size distribution curve), c) $N_2$ adsorption–desorption isotherms of CN/T composites with different ratios and d) BJH pore size distribution curves of CN/T composites with different ratios

As shown in **Figures 4a–c**, the $N_2$ adsorption-desorption isotherms of the synthesized $TiO_2$, CN and CN/T composites all exhibited type IV adsorption curves. According to the IUPAC definition, $TiO_2$, CN, and CN/T composites are all typical mesoporous structures.[31] Both $TiO_2$ and CN/T composites have H2 type hysteresis loops corresponding to ink-bottle type pores.[32] In contrast, the CN hysteresis loop is of the H3 type, indicating the development of slit-shaped structures. The characteristics of isotherms and hysteresis lines are influenced by capillary merging and $TiO_2$ particle clustering inside the structure,[33] aligning with the findings from the SEM analysis. **Table 1** shows the Brunauer-Emmett-Teller (BET) specific surface area of each sample. The results indicate that the specific surface area of the composite increases and then decreases compared to that of the $TiO_2$ monomer after CN is incorporated. Among them, the 7.62 *w*/% CN/T composite exhibits the largest specific surface area.

Moreover, the pore size distributions of monomers $TiO_2$, CN, and CN/T composite appear relatively uniform in the BJH pore size distribution curves displayed in **Figures 4a**, **4b** and **4d**. This homogeneity is a result of the gentle hydrothermal process of program-controlled uniform temperature rise, creating a more uniform internal structure of the catalysts. The increase in the photocatalytic activity of the CN/T composites is probably due to the increase in the BET surface area and the formation of a heterojunction lamellar structure. These modifications expose more active sites on the surface of the 7.62 *w*/% CN/T composite and reduce the carrier migration distance; a larger pore structure allows light to enter the photocatalyst and accelerates the charge transfer. Thus, CN/T composites may have excellent photocatalytic performance.

**Table 1:** BET specific surface area, average pore size, pore volume of $TiO_2$, CN and different components of CN/T composites

| Sample | $S_{BET}$/$m^2 \cdot g^{-1}$ | $D$/nm | $V_{total}$/$cm^3 \cdot g^{-1}$ |
|---|---|---|---|
| $TiO_2$ | 148.95 | 8.22 | 0.432 |
| CN | 34.53 | 13.25 | 0.160 |
| 6.51 *w*/% CN/T | 157.16 | 9.39 | 0.540 |
| 7.62 *w*/% CN/T | 167.35 | 8.56 | 0.516 |
| 8.49 *w*/% CN/T | 161.93 | 9.00 | 0.495 |
| 12.37 *w*/% CN/T | 153.99 | 9.08 | 0.505 |
| 19.60 *w*/% CN/T | 131.83 | 10.53 | 0.481 |

### *3.5 UV–Vis/DRS analysis*

Monomeric CN, $TiO_2$, and different components of CN/T composites were subjected to UV–Vis diffuse reflectance spectroscopy experiments to analyze their optical properties in the UV and visible regions (200–800 nm). **Figure 5a** displays light absorption profiles of different materials, while **Figure 5b** illustrates the energy mapping curves of different samples. **Figure 5a** demonstrates that titanium dioxide exhibits light absorption in a wavelength range of 200–400 nm, likely due to charge transfer from O→Ti, where electrons transition from O 2p orbitals in the valence band (VB) to Ti 3d empty orbitals in the conduction band (CB).[34] Certain light-absorbing characteristics are shown by CN in both

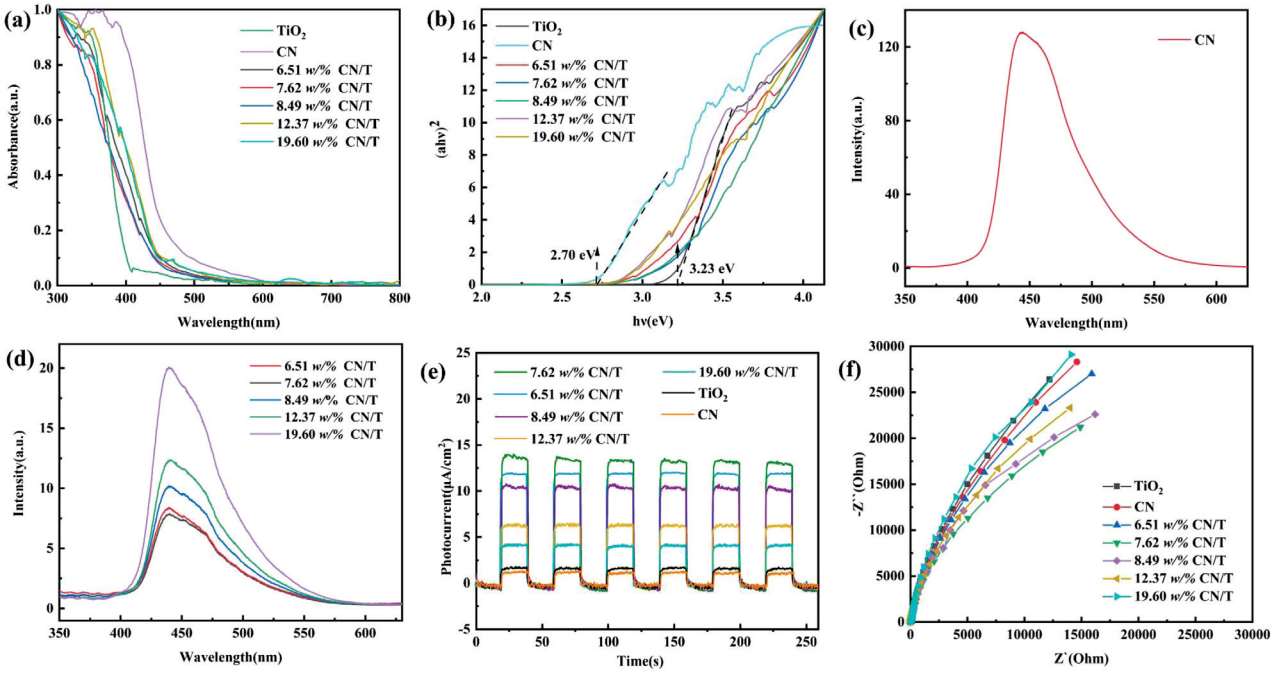


**Figure 5:** UV–Vis/DRS absorption spectra of $TiO_2$, CN and different ratios of CN/T composites (a), Kubelka–Munk energy curve plots of different samples (b), Photoluminescence spectra of CN/T composites with different ratios (c) and CN (d) (Excitation wavelength $\lambda$ = 325 nm), Transient photocurrent response (TPRs) of $TiO_2$, CN and different ratios of CN/T composites (e), and Nyquist plots of $TiO_2$, CN and CN/T (f)

the UV and visible regions; in the latter, its light-absorbing behaviour is noticeably greater than that of monomeric $TiO_2$. In comparison to $TiO_2$, the CN/T composite demonstrates an outstanding visible response, with its light absorption edge shifting into the visible range, situated between CN and $TiO_2$. This phenomenon can be explained by the interplay between CN and anatase $TiO_2$. The photoresponse of the 7.62 *w*/% CN/T composite increased to 460 nm in the visible region.

The forbidden bandwidths of these photocatalysts can be calculated based on Figure 5b and the Kubelka-Munk formula:[35]

$$\alpha h\nu = A\ (h\nu - Eg)^{n/2} \quad (1)$$

where $\alpha$ denotes the absorption coefficient, $h\nu$ denotes the discrete photon energy, A denotes the proportionality constant, $n$ denotes the optical frequency and $Eg$ is the bandgap energy.

As shown in **Figure 5b**, the forbidden bandwidths ranging from 6.51 *w*/% CN/T to 19.60 *w*/% CN/T are 2.95 eV, 3.11 eV, 3.06 eV, 2.92 eV and 2.88 eV. The corresponding forbidden bandwidths of monomeric CN and $TiO_2$ are 2.70 eV and 3.23 eV, respectively. Notably, the band gap of the composite is slightly shifted towards visible light. Compared with monomeric $TiO_2$, the composites are more efficient at separating light-generated electron–hole pairs, resulting in an enhanced photocatalytic activity when exposed to natural light.[36]

### *3.6 Photoluminescence analysis*

To assess the efficacy of the prepared photocatalytic composites for charge carrier separation, a PL analysis was conducted. As shown in **Figure 5c**, the emission peak of monomeric CN in the visible range is approximately 450 nm, aligning with the band gap of CN (2.73 eV).[23] **Figure 5d** shows that the CN/T photocatalytic material has an emission peak similar to CN, while the emission intensity is much lower, indicating that photogenerated charge recombination is restricted. In other words, CN/T composites exhibit a greater photogenerated charge separation efficiency than CN alone. The enhanced efficiency of CN/T in separating photogenerated charges is a result of the built-in electric field created by the heterojunction structure of CN/T hybrids near the interface of CN and $TiO_2$. Among the samples with 6.51 *w*/% CN/T, 7.62 *w*/% CN/T, 8.49 *w*/% CN/T, 12.37 *w*/% CN/T, and 19.60 *w*/% CN/T, the lowest intensity of the PL peak is observed for 7.62 *w*/% CN/T, indicating that the 7.62 *w*/% CN/T composites have the fastest photogenerated electron and hole separation efficiency at the interface.

### *3.7 Electrochemistry analysis*

It is well known that the photovoltaic performance is closely related to the charge carrier transfer and separation ability of photocatalysts. **Figure 5e** shows that different samples exhibit stable photocurrent signals over all six exposure periods of the fast photocurrent response. The order of the instantaneous photocurrent density of different samples is: 7.62*w*/% CN/T > 6.51*w*/% CN/T > 8.49*w*/% CN/T > 12.37*w*/% CN/T > 19.60*w*/% CN/T > $TiO_2$ > CN. Compared to monomeric $TiO_2$ and CN, the increase in the photocurrent density of the CN/T composites indicates that the introduced CN promotes the generation and separation of photogenerated charges. It is noteworthy that 7.62 *w*/% CN/T shows higher photocurrent density, indicating a high photogenerated carrier separation capability. However, an excess of CN may cover the reaction site, which inhibits the migration of photogenerated carriers and ultimately leads to a decrease in the photocurrent intensity, a result that is consistent with the PL emission spectra described above.[37]

To demonstrate the efficiency of photogenerated electron–hole separation and charge transfer, electrochemical impedance spectroscopy (EIS) was performed on $TiO_2$, CN, and CN/T composites. It is clear from **Figure 5f** that the radius of curvatures of CN/T composites decreases and then increases with the incorporation of CN. Among them, the Nyquist plot radius of the curvature of 7.62 *w*/% CN/T is the smallest, which implies that the synthesized 7.62 *w*/% CN/T has the highest charge separation efficiency and lowest charge–transfer resistance. This demonstrates that by preventing electron–hole pairing, the combination of $TiO_2$ and CN can enhance charge transfer in CN/T composites and achieve good photocatalytic performance.

### *3.8 Photocatalytic activity*

Using RhB as a model molecule, a series of multimodal photocatalytic experiments was carried out under UV and simulated sunlight irradiation to investigate the photocatalytic properties of CN/T composites. **Figure 6** shows the effects of the experiment.

**Figure 6a** shows the experimental results of the photocatalytic degradation of RhB in the simulated sunlight mode with different catalysts. The degradation efficiency of the composites in degrading RhB first increased and then decreased with the addition of CN doping following 30 min of simulated sunlight irradiation, in which 7.62 *w*/% CN/T had the highest degradation efficiency compared with the other composites and was twice as high as that of monomeric $TiO_2$. The experimental results confirmed that the photocatalytic activity of $TiO_2$ substantially increased after CN doping. This may additionally be due to the formation of a Z-type heterojunction between $TiO_2$ and CN, which promotes the separation of photogenerated electrons and holes. Nevertheless, the active sites on the surface of the composites decreased and the photocatalytic effect also decreased as the CN loading increased.[36] As shown in **Figure 6c**, the photocatalytic efficiency of CN/T composites under UV light surpasses that of $TiO_2$ and CN. Additionally, with increasing CN doping, the composite mate-

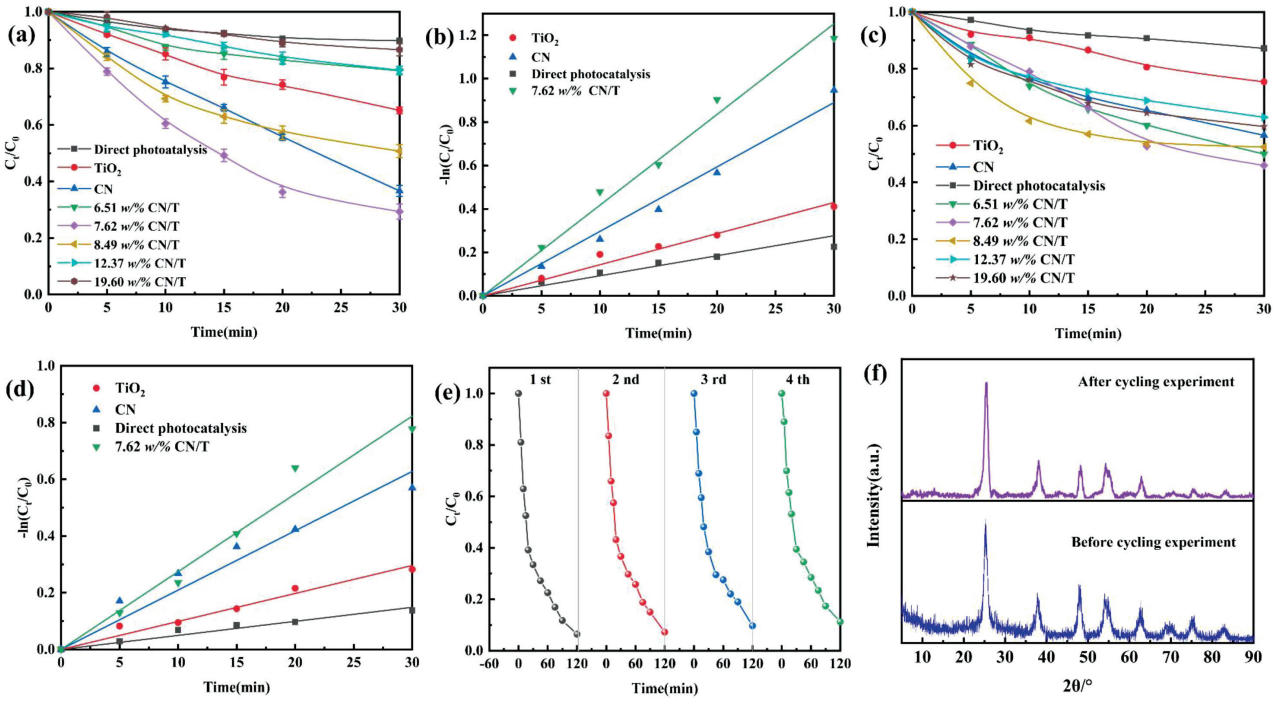


**Figure 6:** Experimental outcome of degradation of RhB in simulated sunlight with different catalysts (a); Reaction kinetics of simulated sunlight catalytic degradation of RhB (b); Experimental outcome of degradation of RhB in UV light with different catalysts (c); Reaction kinetics of UV catalytic degradation of RhB (d); Repeatability tests of 7.62 *w*/% CN/T for four cycles (e); XRD analysis of composites before and after photocatalytic experiments (f)

**Table 2:** Comparison of photocatalytic properties of 7.62 *w*/% CN/T composites with those reported in the literature

| Photocatalyst | Dose (mg) | Pollutant | Dosage (mg/L) | Light irradiation | Irradiation time (min) | Degradation (%) | $K$ ($min^{-1}$) | Ref |
|---|---|---|---|---|---|---|---|---|
| 7.62 *w*/% CN/T | 150 | RhB | 50 | Simulated sunlight<br>UV light | 30<br>30 | 68.58<br>54.05 | 0.042<br>0.027 | Here |
| $Cu_2O$-g-$C_3N_4$ | 10 | TC | 30 | Visible light | 150 | 57.26 | - | [38] |
| $Fe_3O_4$/h$TiO_2$ | 4 | MB | 20 | Simulated sunlight | 120 | 40.30 | 0.004 | [39] |
| Ag/$TiO_2$ | 12 | CAP | 20 | UV light | 120 | 84.00 | 0.006 | [40] |
| CuO–$TiO_2$-2.5-Ag-2 | - | RhB | 5 | UV light | 120 | 91.16 | 0.019 | [41] |
| GO/$TiO_2$ | 200 | MB | 5 | Simulated sunlight | 180 | 99.00 | - | [42] |
| $TiO_2$/GO | 200 | CV | 40 | Simulated sunlight | 120 | 60.00 | 0.006 | [43] |
| $TiO_2$/C-dots/g-$C_3N_4$ | 10 | RhB | 4.79 | UV light | 80 | 83.30 | 0.017 | [44] |
| $Al_2O_3$-$TiO_2$ | 50 | MB | 43 | UV light | 120 | 47.00 | - | [45] |
| 11% Ag/g-$C_3N_4$/CNO-4 | 10 | RhB | 10 | Simulated sunlight | 120 | 82.07 | 0.014 | [46] |
| g-$C_3N_4$/$TiO_2$ | 30 | TA | 10 | Simulated sunlight | 180 | 76.00 | 0.007 | [47] |

rial containing 7.62 *w*/% CN/T demonstrated the highest degradation efficiency for RhB, reaching approximately 55 % in 30 minutes. This efficiency is 2.2 times greater than that of pure $TiO_2$, indicating superior photocatalytic performance. These findings align with the results of UV–Vis diffuse reflectance absorption spectroscopy. The photocatalytic performance of the synthesized 7.62 *w*/% CN/T composite was compared with the results reported in the literature, and the results were shown in **Table 2**.

The first-order reaction model proposed to study the reaction kinetics of the photocatalytic degradation of RhB by $TiO_2$, CN, and CN/T is represented by Equation (2):

$$-\ln (C_t/C_0) = kt \quad (2)$$

where $C_0$ and $C_t$ are the initial concentration at time 0 (the time at which adsorption–desorption equilibrium is reached) and the concentration of RhB dye at time $t$, respectively, while $k$ is the pseudo-primary rate constant.

**Figures 6b** and **6d** show the kinetic profiles of RhB degradation by the catalyst under simulated sunlight and UV light, respectively, indicating that the degradation profiles of the dye molecules by the composites correlate well with the pseudoprimary kinetics; thus, degradation is consistent with the pseudoprimary kinetics. **Figure 6e** displays the results of four consecutive cycle studies measuring the 7.62 *w*/% CN/T degradation of RhB in order to assess the catalyst's stability. The degradation of RhB only decreased by less than 5 % during the four cycles, indicating that the photocatalyst has good cycling

stability. The residual RhB on the surface of 7.62*w*/% CN/T may have led to a slight decrease in its degradation efficiency, thus reducing the active site.[48] In addition, the 7.62 *w*/% CN/T composite before and after cycling was analyzed with XRD in this study. As can be seen in **Figure 6f**, the XRD diffraction peaks of both $TiO_2$ and CN before and after photocatalytic degradation did not exhibit obvious changes, and the composite still had high crystallinity after the photocatalytic experiment, indicating that the 7.62 *w*/% CN/T composite had certain stability.

In order to investigate the degradation effect of 7.62 *w*/% CN/T composite photocatalyst on RhB in different actual water environments, different water bodies (river water, lake water and tap water) were collected for photocatalytic experiments. As can be seen from **Figure 7a**, the removal efficiency of 7.62 *w*/% CN/T composite for RhB was 93.58 % (deionized water), 88.04 % (river water), 62.97 % (tap water), and 51.08 % (lake water). The reduced removal efficiency for RhB in other water sources compared to deionized water was mainly due to the presence of other competing organics, inhibition by co-existing cations and anions, and differences in the pH between different water sources. Therefore, the 7.62 *w*/% CN/T composite has great potential and good applicability in practical wastewater treatment.

### *3.9 Possible photocatalytic reaction mechanism*

To determine a possible mechanism for the photocatalytic degradation of RhB with 7.62 *w*/% CN/T, a capture assay was employed. The findings are displayed in **Figure 7b**. Under the same experimental conditions, photocatalytic capture experiments were conducted using p-benzoquinone (BQ) to capture superoxide radicals ($\cdot O_2^-$), ethylenediamine EDTA-2Na to capture holes ($h^+$), and methanol ($CH_3OH$) to capture hydroxyl radicals (·OH). The degradation rate of RhB decreased when free radical trapping agents were added, indicating that all three active substances,$\cdot O_2^-$, $h^+$ and ·OH, had unique effects on the photodegradation of RhB by CN/T. After the addition of $CH_3OH$, the degradation rate of RhB by 7.62 *w*/% CN/T decreased the most, from 67.56 % to 21.32 %, confirming that ·OH was a primary active ingredient in the photocatalytic process and that it played a significant role in photocatalytic degradation. The degradation rate of the CN/T composites also decreased, notably with the addition of BQ and EDTA, suggesting that the photocatalytic degradation of RhB was influenced in specific ways by $O_2^-$ and $h^+$. This confirmed that $O_2^-$ and $h^+$ acted as supplementary active substances in the photocatalytic process.

The Mott–Schottky plots of monomers $TiO_2$ and CN show positive slopes, indicating the n-type semiconduc-

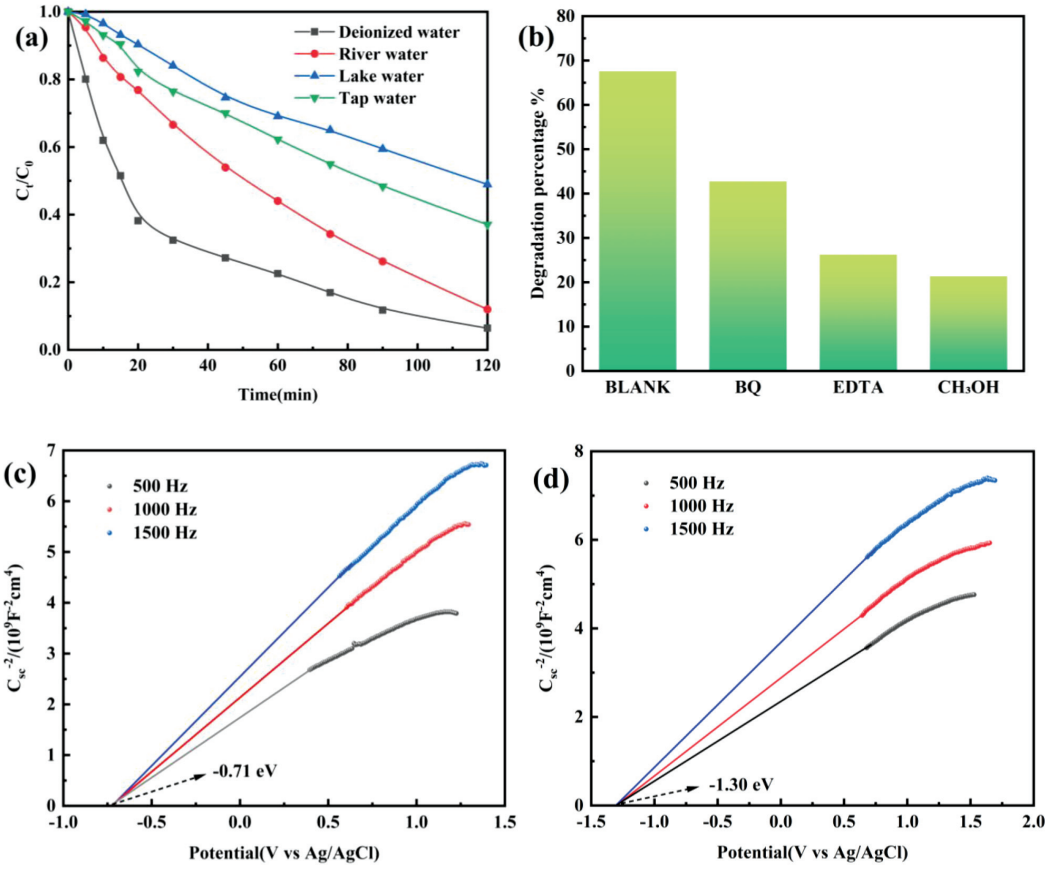


**Figure 7:** a) Photocatalytic degradation of RhB with 7.62*w*/% CN/T composite in different water substrates under simulated sunlight, b) experimental diagram of the capture of 7.62 *w*/% CN/T, c) Mott-Schottky experimental result plots of $TiO_2$ and d) CN

tor nature of the synthesized samples. As shown in **Figures 7c–7d**, the flat band potentials ($E_{FB}$) of $TiO_2$ and CN were derived from the intercepts of the M–S plots on the X-axis, with values of –0.71 eV and –1.30 eV (vs. Ag/AgCl), corresponding to –0.51 eV and –1.10 eV (vs. NHE), respectively. The flat band potential of n-type semiconductors is close to the conduction band (CB) position.[49] Therefore, the conduction band (CB) positions of $TiO_2$ and CN are about –0.51 eV and –1.10 eV (vs. NHE), respectively. Meanwhile, the band gap values of $TiO_2$ and CN are 3.23 eV and 2.70 eV, respectively, from the UV-vis/DRS and Kubelka-Munk energy profile plots. Combined with the equation ($E_{VB} = E_{CB} + E_g$),[50] calculations show that the valence bands of $TiO_2$ and CN are 2.72 eV and 1.60 eV, respectively.

Based on the above experimental results, a possible photocatalytic reaction mechanism for the CN/T system is proposed. If the CN/T heterojunction composites follow the conventional type II charge carrier transfer mechanism (**Figure 8a**), the $e^-$ in the CB of CN is transferred to the CB of $TiO_2$, while the $h^+$ in the VB of $TiO_2$ migrates to the VB of CN. The CB of $TiO_2$ is more negative than the redox potential of $O_2/\cdot O_2^-$ (-0.33 eV vs. NHE), and thus the $e^-$ that accumulates in the CB of $TiO_2$ is energetically sufficient to reduce $O_2$ to form $\cdot O_2^-$ anion radicals. However, $h^+$ accumulated on the VB of CN makes it difficult to oxidize $OH^-/H_2O$ directly to generate OH radicals. Considering the presence of a large number of $\cdot O_2^-$ anion radicals and OH radicals in the CN/T photocatalytic system, the type II charge transfer mechanism is not suitable, so a direct Z-type charge transfer mechanism was proposed (**Figure 8b**).

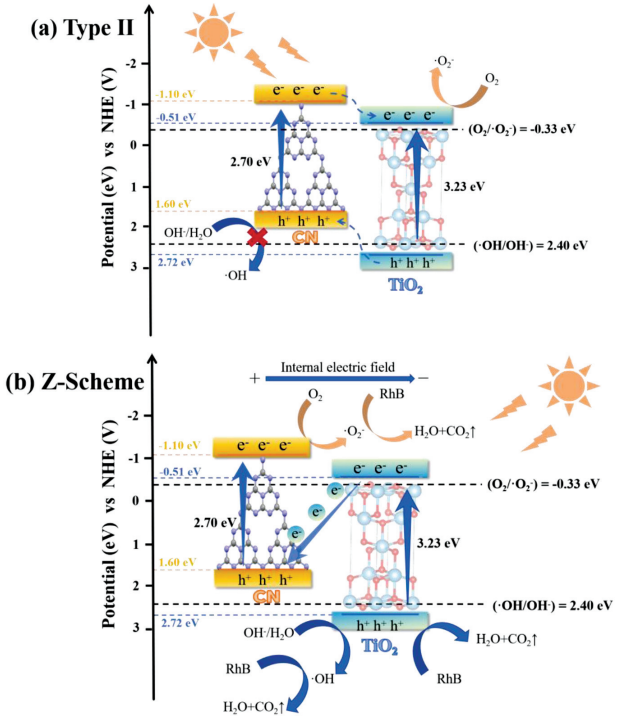


**Figure 8:** Mechanistic diagram of energy band structure arrangement and two possible carrier transfer mechanisms in CN/T heterojunction composites

Under simulated sunlight exposure, the photogenerated electrons undergo a jump and move from the VB to the CB of $TiO_2$. As a result of the heterojunction between CN and $TiO_2$ in the composites, the photogenerated $e^-$ is transferred to the VB of CN to recombine with $h^+$ under the action of the internal electric field. Thus, more reductive photoexcited electrons are retained in the CB of CN, while more oxidized holes are retained in the VB of $TiO_2$. The heterojunction in CN/T accelerates the transfer of photoelectrons and holes generated between CN and $TiO_2$. Since the electron potential in the CB of CN (-1.1 eV) is lower than that in $O_2/\cdot O_2^-$ (-0.33 eV vs. NHE), the electrons accumulated in the CB of CN can reduce $O_2$ molecules to $O_2^-$. Moreover, the hole potential in the VB of $TiO_2$ (2.92 eV) is greater than that in $OH^-/\cdot OH$ (2.40 eV vs. NHE). Consequently, the reaction of $H_2O + h^+ \rightarrow OH$ can occur, where the $h^+$ in the VB of $TiO_2$ reacts with $H_2O$ in the system to form OH.[51] The results show that $O_2^-$ and $h^+$ have strong oxidizing effects and can effectively decompose and mineralize RhB under simulated sunlight.

## 4 CONCLUSION

Heterostructure composites CN/T were synthesized with hydrothermal and sol–gel methods. The layered structure of CN provided sites for $TiO_2$ particles and helped achieve uniform loading of $TiO_2$. The photogenerated electron-hole pair separation efficiency of CN/T composites was greater than that of monomeric CN and $TiO_2$. Among the composites, 7.62 *w*/% CN/T exhibited the most effective photodegradation activity, which was 1.1 and 2 times greater than those of monomeric CN and $TiO_2$, respectively. The 7.62 *w*/% CN/T composite exhibited good absorption and utilization of visible light and therefore the best photocatalytic degradation activity for RhB. This study presents a simple and economical approach to the preparation of CN/T heterostructure composites as photocatalysts; therefore, the synthesized CN/T heterojunction composites may strengthen the solar light utilization of monomeric $TiO_2$.

## Acknowledgments

This study was supported by the National Natural Science Foundation of China (21376126), Heilongjiang Provincial Natural Science Foundation of China (LH2021B031), Key Research and Development Guidance Projects in Heilongjiang Province (GZ20210034), Opening Foundation of Heilongjiang Provincial Key Laboratory of Polymeric Composition Materials (CLKFKT2021B2), Fundamental Research Funds in Heilongjiang Provincial Universities of China (135509104), and Innovation Project of Qiqihar University Graduate Education (QUZLTS_CX2023002).

## 5 REFERENCES


[1] T. Chankhanittha, C. Yenjai, S. Nanan, Utilization of formononetin and pinocembrin from stem extract of Dalbergia parviflora as capping agents for preparation of ZnO photocatalysts for degradation of RR141 azo dye and ofloxacin antibiotic, Catal. Today, 384–386 (**2022**), 279–293, doi:10.1016/j.cattod.2021.03.002

[2] H. F. Wang, Z. C. Li, S. Yahyaoui, H. Hanafy, M. K. Seliem, A. Bonilla-Petriciolet, G. L. Dotto, L. Sellaoui, Q. Li, Effective adsorption of dyes on an activated carbon prepared from carboxymethyl cellulose: experiments, characterization and advanced modelling, Chem. Eng, J. 417 (**2021**) 11, doi:10.1016/j.cej.2020.128116

[3] K. Wannakan, K. Khansamrit, T. Senasu, S. Nanan, Ultrasound-assisted synthesis of a ZnO/$BiVO_4$ S-scheme heterojunction photocatalyst for degradation of the reactive red 141 dye and oxytetracycline antibiotic, ACS Omega, 8 (**2023**), 4835–4852, doi:10.1021/acsomega.2c07020

[4] T. Bayu, H. Kim, T. Oki, Water governance contribution to water and sanitation access equality in developing countries, Water Resour. Res., 56 (**2020**) 13, doi:10.1029/2019WR025330

[5] D. Vaya, P. K. Surolia, Semiconductor based photocatalytic degradation of pesticides: an overview, Environ. Technol. Innov., 20 (**2020**) 25, doi:10.1016/j.eti.2020.101128

[6] Y. W. Zhu, Y. Tian, L. Li, J. Q. Hou, Y. L. Huo, T. Q. Sun, J. X. Li, 3DOM N/$TiO_2$ composite modified by CdS QDs with Z-scheme: enhanced photocatalytic degradation and hydrogen evolution, J. Nanopart. Res., 24 (**2022**) 168, doi:10.1007/S11051-022-05550-Z

[7] G. R. Jia, Y. Wang, X. Q. Cui, W. T. Zheng, Highly carbon-doped $TiO_2$ derived from MXene boosting the photocatalytic hydrogen evolution, ACS Sustain. Chem. Eng., 6 (**2018**), 13480–13486, doi:10.1021/acssuschemeng.8b03406

[8] X. Long, X. B. Wei, Y. H. Qiu, Y. C. Song, L. N. Bi, P. K. Tang, X. B. Yan, S. Z. Wang, J. X. Liao, $TiO_2$ aerogel composite high-efficiency photocatalysts for environmental treatment and hydrogen energy production, Nanotechnol. Rev., 12 (**2023**) 31, doi:10.1515/NTREV-2022-0490

[9] R. Asahi, T. Morikawa, T. Ohwaki, K. Aoki, Y. Taga, Visible-light photocatalysis in nitrogen-doped titanium oxides, Science, 293 (**2001**) 269–271, doi:10.1126/science.1061051

[10] A. E. Mohamed, S. Rohani, Modified $TiO_2$ nanotube arrays (TNTAs): progressive strategies towards visible light responsive photoanode, a review, Energy Environ. Sci., 4 (**2011**), 1065–1086, doi:10.1039/c0ee00488j

[11] J. J. Xian, D. Z. Li, J. Chen, X. F. Li, M. He, Y. Shao, L. H. Yu, J. L. Fang, $TiO_2$ nanotube array-graphene-CdS quantum dots composite film in Z-scheme with enhanced photoactivity and photostability, ACS Appl. Mater. Inter., 6 (**2014**), 13157–13166, doi:10.1021/am5029999

[12] N. Wang, L. Cheng, Y. L. Liao, Q. J. Xiang, Effect of functional group modifications on the photocatalytic performance of CN, Small, 19 (**2023**) 17, doi:10.1002/smll.202300109

[13] L. Zhou, L. Z. Wang, J. L. Zhang, J. Y. Lei, Y. D. Liu, The preparation, and applications of g-$C_3N_4$/$TiO_2$ heterojunction catalysts – a review, Res. Chem. Intermediat., 43 (**2017**), 2081–2101, doi:10.1007/s11164-016-2748-8

[14] S. H. Liu, C. L. Wang, Y. Song, B. L. Yan, B. Ai, K. F. Pan, L. P. Zhang, Fabrication of a hybrid phase $TiO_2$/g-$C_3N_4$ heterojunction composite with enhanced adsorption and photocatalytic degradation of MB under visible light, New J. Chem., 47 (**2023**), 8170–8181, doi:10.1039/d3nj00926b

[15] Z. A. Huang, Q. Sun, K. Lv, Z. Zhang, M. Li, B. Li, Effect of contact interface between $TiO_2$ and g-$C_3N_4$ on the photoreactivity of g-$C_3N_4$/$TiO_2$ photocatalyst: (001) vs (101) facets of $TiO_2$, Appl. Catal. B: Environ., 164 (**2015**), 420–427, doi:10.1016/j.apcatb.2014.09.043

[16] H. Li, X. Wu, S. Yin, K. Katsumata, Y. Wang, Effect of rutile $TiO_2$ on the photocatalytic performance of CN/brookite-$TiO_{2-x}N_y$ photocatalyst for NO decomposition, Appl. Surf. Sci., 392 (**2017**), 531–539, doi:10.1016/j.apsusc.2016.09.075

[17] R. Acharya, K. Parida, A review on $TiO_2$/g-$C_3N_4$ visible-light-responsive photocatalysts for sustainable energy generation and environmental remediation, J. Environ. Chem. Eng., 8 (**2020**) 21, doi:10.1016/j.jece.2020.103896

[18] X. J. Wen, Q. Lu, X. X. Lv, J. Sun, J. Guo, Z. H. Fei, C. G. Niu, Photocatalytic degradation of sulfamethazine using a direct Z-Scheme AgI/$Bi_4V_2O_{11}$ photocatalyst: Mineralization activity, degradation pathways and promoted charge separation mechanism, J. Hazard. Mater., 385 (**2020**), 121508, doi:10.1016/j.jhazmat.2019.121508

[19] J. Sun, C. H. Shen, J. Guo, H. Guo, Y. F. Yin, X. J. Xu, Z. H. Fei, Z. T. Liu, X. J. Wen, Highly efficient activation of peroxymonosulfate by $Co_3O_4$/$Bi_2WO_6$ p-n heterojunction composites for the degradation of ciprofloxacin under visible light irradiation, J. Colloid Interface Sci., 588 (**2021**), 19–30, doi:10.1016/j.jcis.2020.12.043

[20] J. Guo, C. H. Shen, J. Sun, X. J. Xu, X. Y. Li, Z. H. Fei, Z. T. Liu, X. J. Wen, Highly efficient activation of peroxymonosulfate by $Co_3O_4$/$Bi_2MoO_6$ p-n heterostructure composites for the degradation of norfloxacin under visible light irradiation, Sep. Purif. Technol., 259 (**2021**), 118109, doi:10.1016/j.seppur.2020.118109

[21] C. H. Shen, Y. Chen, X. J. Xu, X. Y. Li, X. J. Wen, Z. T. Liu, R. Xing, H. Guo, Z. H. Fei, Efficient photocatalytic $H_2$ evolution and Cr (VI) reduction under visible light using a novel Z-scheme $SnIn_4S_8$/$CeO_2$ heterojunction photocatalysts, J. Hazard. Mater., 416 (**2021**), 126217, doi:10.1016/J.JHAZMAT.2021.126217

[22] B. Gao, J. Wang, M. Dou, C. Xu, X. Huang, Enhanced photocatalytic removal of amoxicillin with Ag/$TiO_2$/mesoporous CN under visible light: property and mechanistic studies, J. Environ. Sci. Pollut. R., 27 (**2020**), 7025–7039, doi:10.1007/s11356-019-07112-8

[23] S. Zhao, S. Chen, H. Yu, Q. Xie, g-$C_3N_4$/$TiO_2$ hybrid photocatalyst with wide absorption wavelength range and effective photogenerated charge separation, J. Sep. Purif. Technol., 99 (**2012**), 50–54, doi:10.1016/j.seppur.2012.08.024

[24] H. Tang, S. Chang, L. Jiang, G. Tang, W. Liang, Novel spindle-shaped nanoporous $TiO_2$ coupled graphitic g-$C_3N_4$ nanosheets with enhanced visible-light photocatalytic activity, J. Ceram. Int., 42 (**2016**), 18443–18452, doi:10.1016/j.ceramint.2016.08.179

[25] M. L. Matias, A. S. R. Machado, J. Rodrigues, T. Calmeiro, J. Deuermeier, A. Pimentel, E. Fortunato, R. Martins, Microwave Synthesis of Visible-Light-Activated g-$C_3N_4$/$TiO_2$ Photocatalysts, Nanomaterials, 13 (**2023**), 1090, doi:10.3390/nano13061090

[26] W. Wang, H. Zhou, Y. Liu, S. Zhang, Y. Zhang, G. Wang, H. Zhang, H. Zhao, Formation of BNC coordination to stabilize the exposed active nitrogen atoms in g-$C_3N_4$ for dramatically enhanced photocatalytic ammonia synthesis performance, Small, 16 (**2020**), e1906880, doi:10.1002/smll.201906880

[27] X. Y. Wang, J. Q. Meng, X. Y. Zhang, Y. Q. Liu, M. Ren, Y. X. Yang, Y. H. Guo, Controllable approach to carbon-deficient and oxygen-doped graphitic carbon nitride: Robust photocatalyst against recalcitrant organic pollutants and the mechanism insight, J. Adv. Funct. Mater., 31 (**2021**), 2010763, doi:10.1002/adfm.202010763

[28] Y. C. Cao, G. Q. Yuan, Y. Guo, X. L. Hu, G. Z. Fang, S. Wang, Facile synthesis of $TiO_2$/g-$C_3N_4$ nanosheet heterojunctions for efficient photocatalytic degradation of tartrazine under simulated sunlight, J. Appl. Surf. Sci., 600 (**2022**), 54169, doi:10.1016/j.apsusc.2022.154169

[29] M. Nawaz, W. Miran, J. Jang, D. S. Lee, Stabilization of Pickering emulsion with surface-modified titanium dioxide for enhanced photocatalytic degradation of Direct Red 80, J. Catal. Today, 282 (**2017**), 38–47, doi:10.1016/j.cattod.2016.02.017

[30] B. Kholikov, J. Hussain, H. Zeng, Gold modifed $TiO_2$/g-$C_3N_4$ for enhanced photocatalytic activities to evolved $H_2$ fuel, J. Inorg. Chem. Commun., 6 (**2021**), 108787, doi:10.1016/j.inoche.2021.108787

[31] A. A. Alothman, A. Ayub, S. K. Hachim, B. M. Mohammed, F. Hussain, M. Altaf, Z. J. Kadhim, H. A. Lafta, Y. S. Alnassar, M. A. Shams, N. A. Almuhous, M. Ouladsmane, M. Sillanpaa, Facile syn-

thesis and comparative study of the enhanced photocatalytic degradation of two selected dyes by $TiO_2$-g-$C_3N_4$ composite, J. Environ. Sci. Pollut. R., 30 (**2022**), 37332–37343, doi:10.1007/s11356-022-24839-z

[32] K. S. W. Sing, Reporting physisorption data for gas/solid systems with special reference to the determination of surface area and porosity (Recommendations 1984), J. Pure. Appl. Chem., 57 (**1985**), 603–619, doi:10.1351/pac198557040603

[33] Q. Zhou, L. Li, Z. Xin, Y. Yu, L. Wang, W. Zhang, Visible light response and heterostructure of composite CdSŽZnS-ZnO to enhance its photocatalytic activity, J. Alloys Compd., 813 (**2019**), 152–190, doi:10.1016/j.jallcom.2019.152190

[34] Y. Liu, M. Ren, X. Zhang, G. Yang, L. Qin, J. Meng, Y. Guo, Supramolecule self-assembly approach to direct Z-scheme $TiO_2$/g-$C_3N_4$ heterojunctions for efficient photocatalytic degradation of emerging phenolic pollutants, J. Appl. Surf. Sci., 593 (**2022**), 153401, doi:10.1016/J.APSUSC.2022.153401

[35] W. Zhao, Y. Guo, Y. Faiz, W. T. Yuan, C. Sun, S. M. Wang, Y. H. Deng, Y. Zhuang, Y. Li, X. M. Wang, Facile in-suit synthesis of Ag/$AgVO_3$ one-dimensional hybrid nanoribbons with enhanced performance of plasmonic visible-light photocatalysis, J. Appl. Catal. B: Environ., 163 (**2015**), 288–297, doi:10.1016/j.apcatb.2014.08.015

[36] Y. J. Zhang, X. C. Ren, L. H. Yang, Z. Y. Chen, Z-scheme $TiO_2$/g-$C_3N_4$ composites prepared by hydrothermal assisted thermal polymerization with enhanced visible light photocatalytic activity, J. Res. Chem. Intermediat., 47 (**2021**), 1503–1518, doi:10.1007/s11164-020-04379-2

[37] M. Q. Tian, J. J. Wang, R. J. Sun, D. Z. Lu, N. Li, T. J. Liu, M. Yao, G. Q. Zhang, L. B. Li, Facile synthesis of rod-like $TiO_2$-based composite loaded with g-$C_3N_4$ for efficient removal of high-chroma organic pollutants based on adsorption-photocatalysis mechanism, Inorg. Chem. Commun., 141 (**2022**), 109517, doi:10.1016/j.inoche.2022.109517

[38] H. B. Xiong, K. N. Yin, L. L. Wang, J. Wang, Z. B. Hai, Obvious enhancement of visible photocatalytic performance of $Cu_2O$ modified with $TiO_2$-g-$C_3N_4$: A strategy to achieve synergistic effect of p-n junction and Z-scheme, Opt. Mater., 138 (**2023**), 113727, doi:10.1016/j.optmat.2023.113727

[39] X. Li, W. L. Zhang, X. J. Wen, L. J. You, J. M. Li, Construction of magnetically recyclable $Fe_3O_4$/h$TiO_2$/g-$C_3N_4$ composites for solar photocatalytic degradation of organic pollutants: Study on the performance and mechanism insight, J. Mol. Liq., 392 (**2023**), 123498, doi:10.1016/j.molliq.2023.123498

[40] A. Jodat, A. Jodat, Photocatalytic degradation of chloramphenicol and tartrazine using Ag/$TiO_2$ nanoparticles, Desalin. Water Treat., 52 (**2014**), 13–15, doi:10.1080/19443994.2013.794115

[41] L. Zhang, J. Y. Yang, H. Z. Ma, Ag-Decorated Chrysanthemum-Like CuO–$TiO_2$ Thin Film: Enhanced Photocatalytic Degradation of Rhodamine B, Phys. Status Solidi A, 221 (**2024**) 7, doi:10.1002/pssa.202300599

[42] A. K. Tonni, M. T. Zhu, F. Dun, K. Y. Swee, H. D. O. Mohd, A. Ram, O. Y. Tong, Functionalizing $TiO_2$ with graphene oxide for enhancing photocatalytic degradation of methylene blue (MB) in contaminated wastewater, J. Environ. Manage., 270 (**2020**) 15, doi:10.1016/j.jenvman.2020.110871

[43] M. Sharma, K. Behl, S. Nigam, M. Joshi, $TiO_2$-GO nanocomposite for energy and environmental applications: A green synthesis approach, Vacuum, 156 (**2018**), 434–439, doi:10.1016/j.vacuum.2018.08.009

[44] Z. Y. Chen, T. H. Ji, Z. M. Xu, P. Y. Guan, D. J. Jv, Hydrothermally activated $TiO_2$ nanoparticles with a C-dot/g-$C_3N_4$ heterostructure for photocatalytic enhancement, Nanoscale Adv., 3 (**2021**), 4089–4097, doi:0.1039/D1NA00213A

[45] C. Karunakarana, P. Magesanb, P. Gomathisankarc, P. Vinayagamoorthy, Photocatalytic degradation of dyes by $Al_2O_3$-$TiO_2$ and $ZrO_2$-$TiO_2$ nanocomposites, Mater. Sci. Forum, 734 (**2012**), 325–333, doi:10.4028/www.scientific.net/MSF.734.325

[46] F. G. Yang, H. W. Zhang, Q. Tang, S. H. Lu, H. S. Zhang, X. H. Zheng, Z-scheme Ag-loaded g-$C_3N_4$/$CuNb_2O_6$ composite photocatalyst for RhB dye degradation, Res. Chem. Intermed., 48 (**2022**), 4163–4182, doi:10.1007/s11164-022-04812-8

[47] R. Ratshiedana, P. J. Mafa, O. J. Fakayode, A. K. Mishra, A. T. Kuvarega, Ag doped $TiO_2$ anchored on metal free g-$C_3N_4$ for enhanced solar light activated photodegradation of a dye, Opt. Mater., 157 (**2024**), 116125, doi:10.1016/j.optmat.2024.116125

[48] R. Liu, X. Han, R. Liu, Z. Qi, B. Q. Ren, Y. Sun, Molecularly imprinted $Fe_3O_4$/g-$C_3N_4$/$TiO_2$ catalyst for selective photodegradation of chlorotetracycline, Colloid Surface A, 680 (**2024**), 132691, doi:10.1016/j.colsurfa.2023.132691

[49] C. J. Wang, X. Liu, W. J. He, Y. L. Zhao, Y. C. Wei, J. Xiong, J. Liu, J. M. Li, W. Y. Song, X. Zhang, Z. Zhao, All-solid-state Z-scheme photocatalysts of g-$C_3N_4$/Pt/macroporous-($TiO_2$@carbon) for selective boosting visible-light-driven conversion of $CO_2$ to $CH_4$, J. Catal., 389 (**2020**), 440–449, doi:10.1016/j.jcat.2020.06.026

[50] S. S. Ren, J. H. Dong, X. Y. Duan, T. T. Cao, H. B. Yu, Y. Lu, D. D. Zhou, A novel (Zr/Ce) UiO-66 ($NH_2$) @g-$C_3N_4$ Z-scheme heterojunction for boosted tetracycline photodegradation via effective electron transfer, Chem. Eng. J., 460 (**2023**), 141884, doi:10.1016/j.cej.2023.141884

[51] W. Wang, J. Fang, S. Shao, M. Lai, C. Lu, Compact and uniform $TiO_2$@g-$C_3N_4$ core-shell quantum heterojunction for photocatalytic degradation of tetracycline antibiotics, Appl. Catal. B: Environ., 217 (**2017**), 57–64, doi:10.1016/j.apcatb.2017.05.037